Bridging Charge-Orbital Ordering and Fermi Surface Instabilities in Half-Doped Single-Layered Manganite $La_{0.5}Sr_{1.5}MnO_4$

D. V. Evtushinsky,[1] D. S. Inosov,[1,2] G. Urbanik,[1,3] V. B. Zabolotnyy,[1] R. Schuster,[1] P. Sass,[1] T. Hänke,[1] C. Hess,[1] B. Büchner,[1] R. Follath,[4] P. Reutler,[5] A. Revcolevschi,[5] A. A. Kordyuk,[1,6] and S. V. Borisenko[1]

[1]*Institute for Solid State Research, IFW Dresden, Post Office Box 270116, D-01171 Dresden, Germany*
[2]*Max-Planck-Institute for Solid State Research, Heisenbergstrasse 1, D-70569 Stuttgart, Germany*
[3]*Institute of Experimental Physics, University of Wroclaw, pl. Maxa Borna 9, 50-204 Wroclaw, Poland*
[4]*BESSY GmbH, Albert-Einstein-Strasse 15, 12489 Berlin, Germany*
[5]*Laboratoire de Physico-Chimie de l'Etat Solide, Université Paris-Sud XI, 91405 Orsay Cédex, France*
[6]*Institute of Metal Physics of National Academy of Sciences of Ukraine, 03142 Kyiv, Ukraine*

(Received 2 December 2008; revised manuscript received 25 June 2010; published 28 September 2010)

The single-layered half-doped manganite $La_{0.5}Sr_{1.5}MnO_4$ (LSMO), was studied by means of the angle-resolved photoemission spectroscopy (ARPES), scanning tunneling microscopy (STM), and resistivity measurements. STM revealed a smooth reconstruction-free surface; the density of states, extracted from photoemission and tunneling spectroscopy, is in agreement with transport measurements. The derived from ARPES Fermi surface (FS) nesting properties correspond to the known pattern of the charge-orbital ordering (COO), which implies that FS instability is related to the propensity to form a COO state in LSMO.

DOI: 10.1103/PhysRevLett.105.147201 PACS numbers: 75.47.Lx, 68.37.Ef, 74.25.Jb, 79.60.−i

Density waves are inherent to the phase diagrams of materials that exhibit unusual, and sometimes extraordinarily useful properties, such as superconductivity and colossal magnetoresistance [1–4]. The well-known pure charge ordering, commonly referred to as charge density waves (CDW), is well described by an itinerant approach [5,6], where electrons are treated as waves propagating through a crystal. The charge-orbital ordering (COO) is usually explained by a local approach [7], where the electrons are treated as localized on the atomic sites. On the other hand, several theoretical papers appeared recently, suggesting that description of the COO phenomenon is also possible in an itinerant approach [8]. This situation reflects general dilemma of choice between real and reciprocal space as a starting basis. In general, both approaches should lead to the same results, although it remains unclear, which of them will provide the most comprehensive and transparent understanding of the COO physics.

Here we present an experimental investigation of the half-doped single-layered manganite $La_{0.5}Sr_{1.5}MnO_4$ (LSMO), a renown representative of manganites, which exhibits a prominent transition to the COO state [9–12], by two complementary powerful experimental techniques, a real-space probe, scanning tunneling microscopy (STM), and a reciprocal-space probe, angle-resolved photoemission spectroscopy (ARPES). The momentum-resolved electronic structure of LSMO is extracted from the ARPES data for the first time. The electronic susceptibility, calculated on the basis of the revealed band dispersion, exhibits a prominent nesting-driven peak at one quarter of the Brillouin zone diagonal, that is equal to the reciprocal lattice vector of the charge-orbital pattern. Our results demonstrate intimate relation between the Fermi surface (FS) geometry and the propensity of the system to form a COO state which, in turn, implies the possibility of straightforward description of the COO in the itinerant approach.

A typical STM topographic image obtained on an *in situ* cleaved surface of the manganite, is shown in Fig. 1(b). The measured step heights are equal to $n \times (0.62 \pm 0.02)$ nm, $n \in \mathbb{Z}$, that is a multiple of half the **c** lattice constant [Fig. 1(c)]. This implies that the cleavage takes place between the adjacent La,Sr oxide layers [Fig. 1(a)]. In contrast to Ref. [13], our data reveal well resolved surfaces and steps, both above and below the COO temperature, $T_{COO} = 230$ K. The measured roughness of the terraces, observed in our data, was usually 0.1 nm, indicating previous assessments (0.6 nm) [11,13] to be largely overestimated. A large defect-free portion of the surface is shown in Fig. 1(d), where the atomically resolved topography is highlighted by the Fourier transform of the STM image [Fig. 1(e)]. The absence of additional peaks in low-energy electron diffraction (LEED) image [Fig. 1(f)] confirms the absence of any significant surface reconstruction. Figure 1(g) shows a higher-magnified image with a superimposed cartoon of the crystalline structure.

In Fig. 2(a) we show both, photoemission and tunneling spectra taken from the surface discussed above. The extracted densities of states (DOS), shown on the same energy scale, exhibit similar behavior near the Fermi level. This semiconducting behavior is in agreement with the temperature dependence of the in-plane resistivity ρ, which is linear in $\ln\rho$ versus $1/T$ coordinates [Fig. 2(b)] [14]. The values of the energy gap, determined from the resistivity measurements ($\Delta_1 = 136$ meV above and

$\Delta_2 = 255$ meV below T_{COO} respectively), are consistent with our spectroscopic data. Resistivity shows a sharp transition at T_{COO}, indicating good crystal quality, while ARPES and STS data indicate rather smooth shift of the spectral weight away from the Fermi level with cooling. As shown in the supplementary materials [16], charging effects, which generally are to be taken into account when measuring poorly conducting samples, are negligible for relevant temperature range. Also a smeared COO transition on the surface was found in the comparative x-ray scattering studies of bulk and surface of the same material [11].

Now we turn to the reciprocal-space image of the LSMO electronic structure. In Figs. 3(a)–3(e) we present ARPES intensity maps. In the following we will refer to these maps as remnant Fermi surface [15]. Since the energy gap, estimated from both spectroscopic and transport data, is rather small in comparison with the bandwidth, the remnant FS is very close to the hypothetical FS of the nongapped parent metal [17] and thus has similar properties. As for each particular excitation energy the photoemission matrix elements highlight and suppress different parts of the spectrum [18,19], which may lead to false conclusions as for the geometry of the electronic structure, we carried out the series of measurements at different photon energies and light polarizations, also analyzing data taken in different Brillouin zones [Figs. 3(a)–3(e)]. The compilation of the data allows us to conclude that the remnant FS of LSMO consists of a large holelike barrel centered at the K point and a small electronlike pocked centered at the Γ point, just as in bilayer manganites in their metallic state [20,21]. We found that the band dispersion, forming remnant FS sheets is well described by the following tight-binding formula:

$$\begin{aligned}\varepsilon(k_x, k_y) = {} & d_0 + d_1(\cos k_x a + \cos k_y a) \\ & + d_2 \cos k_x a \cos k_y a + d_3(\cos 2k_x a + \cos 2k_y a) \\ & + d_4(\cos 2k_x a \cos k_y a + \cos k_x a \cos 2k_y a) \\ & + d_5 \cos 2k_x a \cos 2k_y a \ [\mathrm{eV}] \end{aligned} \quad (1)$$

with $d_0 = 3.050$, $d_1 = -4.638$, $d_2 = 3.022$, $d_3 = 1.006$, $d_4 = -1.720$, $d_5 = 0.660$ for the K barrel, and $d_0 = 5.33$, $d_1 = -2.974$, $d_2 = 0$, $d_3 = 0$, $d_4 = 0$, $d_5 = 0$ for the Γ pocket, where $a = 3.865$ Å [12] is a lattice constant [22,23]. It is interesting, that the area enclosed by the contours (49% of the Brillouin zone) is close to the half-filling and since this will not change much in the absence of the energy gap [17], this is in contrast to the nominal doping level of 1/2 electron per Mn atom, which corresponds to 25% of the Brillouin zone. Here we also note, that at particular polarizations and excitation energies an apparent anisotropy of the photoemission signal shows up [see, e.g., Figs. 3(c) and 3(e)], which might point to the sample anisotropy in the a-b plane [24]. However, rotation of the sample by 90° did not affect the measured signal, so we may conclude that the mentioned anisotropy of the spectra arises purely from the anisotropy of the photoemission matrix elements. The absence of any inherent sample anisotropy both above and below T_{COO} is in agreement with the presence of small domains with different orientations of the COO pattern [25], see Figs. 4(a) and 4(b).

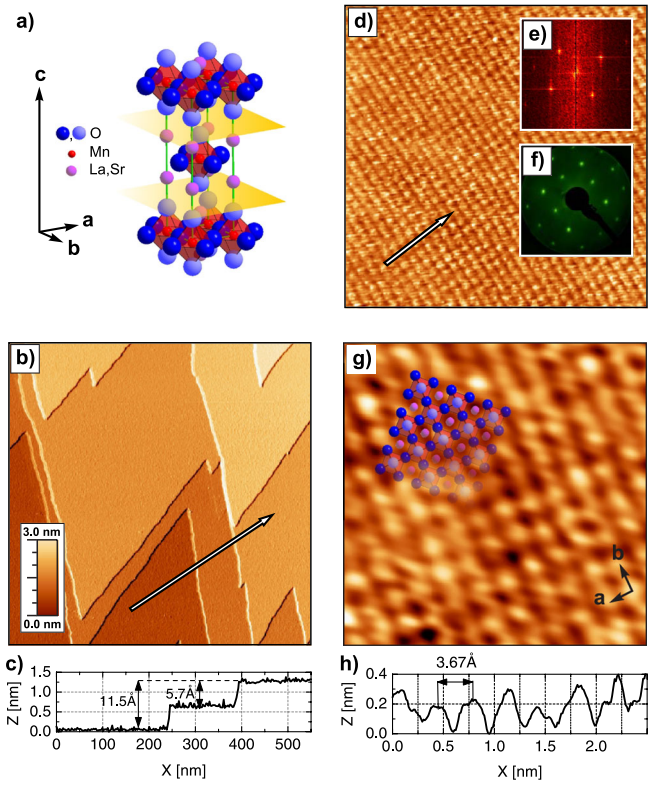

FIG. 1 (color online). (a) The elementary cell and cleavage planes of $La_{0.5}Sr_{1.5}MnO_4$. (b) 1 μm × 1 μm image of atomically flat micrometer-sized terraces separated by steps. (c) The line profile measured on the (b), highlighting half-unit-cell high steps. (d) 10 nm × 10 nm atomic-resolution image measured on the flat terrace from (b). (e) The Fourier transform of the STM image (d). (f) LEED image, taken at 100 eV with the same orientation as the STM image, indicates a reconstruction-free surface. (g) Higher-magnification image of an area from the (d). (h) The line profile measured on the (d), showing the atomic modulations. STM topographic images, taken at 300 K.

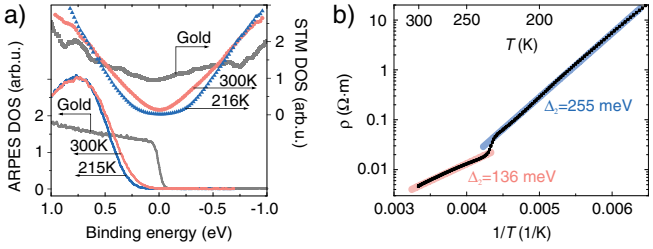

FIG. 2 (color online). (a) The DOS extracted from the tunneling (averaged over a whole momentum space) and photoemission (Γ pocket) data above and below T_{COO}. Spectroscopies on gold are shown for calibration. (b) $\ln\rho$ plotted versus $1/T$ with linear fit above and below T_{COO}.

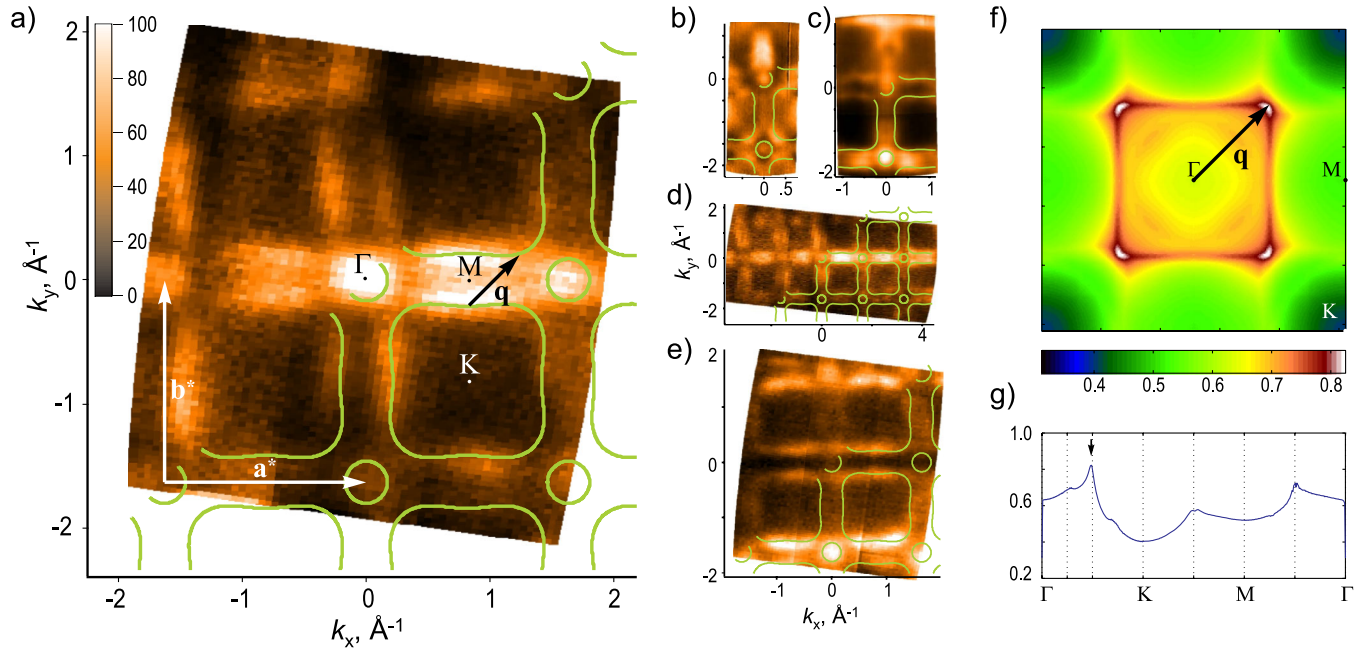

FIG. 3 (color online). The photoemission intensity, integrated in energy window of 70 meV width, centered at 190 meV below Fermi level, is shown in panels (a)–(e) for different excitation energies and light polarizations: (a) linear horizontal, 157 eV, 300 K; (b) linear horizontal, 37 eV, 190 K; (c) linear horizontal, 70 eV, 195 K; (d) linear horizontal, 200 eV, 300 K; (e) linear vertical, 157 eV, 300 K. Contours of the remnant Fermi surface, which consists of a small round electronlike pocket centered at the Γ point and a large square holelike barrel centered at the *K* point, are presented in panels (a)–(e) by green lines. The calculated susceptibility is shown in panel (f), and its profile along the high-symmetry directions is shown in (g).

With the LSMO electronic structure at hand we try to understand the origin of the charge-orbital ordering in this compound in the framework of an itinerant approach. Thereto we refer to the experience gained from studying compounds that exhibit another type of ordering—charge density wave. In these compounds, the major reason that drives the formation of the ordering is well understood: if the electronic susceptibility (Lindhard function) of the *unreconstructed* system possesses a strong peak at a particular wave vector, the system is likely to develop a density wave order at this vector [5,6]. On the basis of the band dispersion extracted from ARPES data we have calculated the susceptibility of the hypothetical LSMO metal by a procedure similar to that described in Ref. [26]. The result of these calculations is shown in Figs. 3(f) and 3(g). The susceptibility turns out to have a prominent nesting-driven peak very close to the vector $\mathbf{q} = \mathbf{a}^*/4 + \mathbf{b}^*/4$, where $\mathbf{a}^* = 2\pi\mathbf{a}/|\mathbf{a}|^2$ and $\mathbf{b}^* = 2\pi\mathbf{b}/|\mathbf{b}|^2$ are the lattice vectors in the reciprocal (momentum) space, while $\mathbf{a}$ and $\mathbf{b}$ are lattice vectors in the direct (coordinate) space [27]. Generally speaking, the FS nesting occurs when two replicas with opposite Fermi velocities meet each other. It means that the nesting is strong when FS sheets of the same origin (both holelike or both electronlike) are externally tangent, or when the FS sheets of different origin (one holelike and another electronlike) are internally tangent. In Fig. 4(c), FS (green solid line) and its replica shifted by the vector $\mathbf{q}$ (orange thin line) are shown [panel (d) corresponds to a different orientation of the charge-orbital pattern]. We see that the FS of LSMO is nested with the vector $\mathbf{q}$—there are two regions that contribute mostly to the peak in the susceptibility: the electronlike Γ-pocket fits inside the rounded corner of the square-shaped holelike barrel, and the convex corner of the holelike barrel fits inside its concave part [28]. It is particularly important that nesting should be present in the unreconstructed, ''initial'' system, as partial or complete gapping of the FS due to the formation of the order does not lead to any significant change of the peak position in the electronic susceptibility [29,30]. In such case the gain in electronic energy comes from further opening of already present gap, although for the reconstructed FS nesting in its conventional sense is destroyed.

In conclusion, the found nesting vector, $\mathbf{q} = \mathbf{a}^*/4 + \mathbf{b}^*/4$, is reciprocal to the lattice vector of the charge-orbital superstructure [Fig. 4(a)], directed along zigzag chains, $\boldsymbol{\lambda} = 2\mathbf{a} + 2\mathbf{b}$ [4], which hints that the formation of COO state in $La_{0.5}Sr_{1.5}MnO_4$ is connected to the FS instability due to the nesting-driven peak in the electronic susceptibility. Albeit some theoretical works have predicted a possibility of the description of the COO phenomena via the band approach [8] (which would allow to bridge COO with many other cases of superstructure formation [1,2,5,6,31–34]) as an alternative to the existing local approach [7], no relation between the COO origin and the fermiology has been established to date to our knowledge. Our observations provide such a link by suggesting that FS instabilities can serve as a possible origin of the

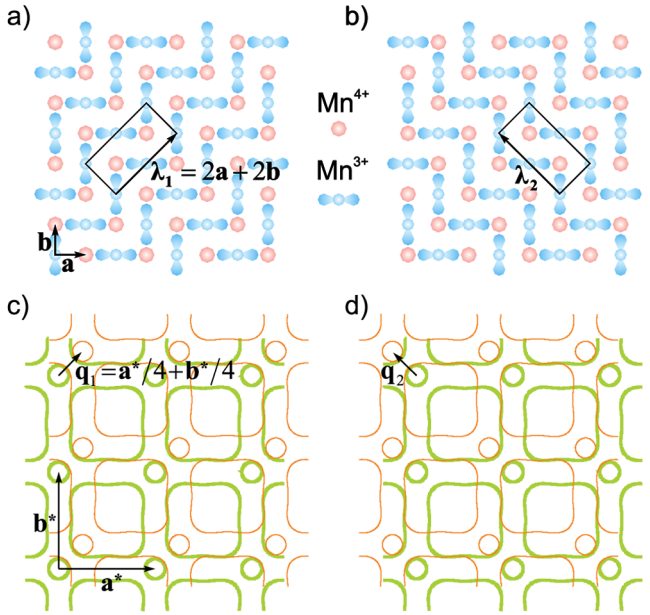

FIG. 4 (color online). The modulation in direct space and the corresponding nesting in reciprocal space; illustration of two possible orientations of the charge-orbital pattern. (a), (b) Real-space pattern of the charge-orbital order with superlattice vectors $\boldsymbol{\lambda}_{1,2} = \pm 2\mathbf{a} + 2\mathbf{b}$ along zigzags. (c), (d) Fermi surface (green solid lines) and its replicas (thin orange lines) displaced by the vectors $\mathbf{q}_{1,2} = \pm \mathbf{a}^*/4 + \mathbf{b}^*/4$. Note that the observed nesting vector, $\mathbf{q}_{1,2}$ corresponds to the periodicity of the charge-orbital pattern along zigzags, $\boldsymbol{\lambda}_{1,2}$: $|\mathbf{q}_{1,2}| = (2\sqrt{2})^{-1}|\mathbf{a}^*|$, $|\boldsymbol{\lambda}_{1,2}| = 2\sqrt{2}|\mathbf{a}|$, and $\mathbf{q}_{1,2} \parallel \boldsymbol{\lambda}_{1,2}$.

COO. From a broader perspective, although the critical temperature of the transition to the ordered state as well as the strength of the band reconstruction are dependent on the coupling to a mediator, the periodicity of the modulation seems to be determined by the electronic band geometry in most cases of superstructure formation: CDW in transition metal chalcogenides [1,6,35,36], magnetic ordering in ternary rare earth silicides [31], spin density wave in iron pnictides [32], a hidden order in cuprates [2,33], etc.

The project is part of the FOR538 and was supported by the DFG under Grants No. KN393/4 and BO1912/2-1. We thank A. M. Gabovich for useful discussions, R. Hübel for technical support, and A. Narduzzo and R. Schneider for resistivity measurements. ARPES experiments were performed using the "1^3 ARPES" end station at BESSY synchrotron in Berlin (Helmholtz-Zentrum für Materialien und Energie).

[1] E. Morosan *et al.*, Nature Phys. **2**, 544 (2006).
[2] T. Hanaguri *et al.*, Nature (London) **430**, 1001 (2004).
[3] G. C. Milward *et al.*, Nature (London) **433**, 607 (2005).
[4] Y. Tokura and N. Nagaosa, Science **288**, 462 (2000).
[5] S.-K. Chan and V. Heine, J. Phys. F **3**, 795 (1973); J. A. Wilson, Phys. Rev. B **15**, 5748 (1977).
[6] S. V. Borisenko *et al.*, Phys. Rev. Lett. **100**, 196402 (2008); Phys. Rev. Lett. **102**, 166402 (2009); D. S. Inosov *et al.*, New J. Phys. **10**, 125027 (2008).
[7] J. van den Brink, G. Khaliullin, and D. Khomskii, Phys. Rev. Lett. **83**, 5118 (1999).
[8] S. Yarlagadda *et al.*, Phys. Rev. B **80** 235123 (2009); D. V. Efremov and D. I. Khomskii, Phys. Rev. B **72**, 012402 (2005).
[9] Y. Moritomo *et al.*, Phys. Rev. B **51**, 3297 (1995).
[10] D. Senff *et al.*, Phys. Rev. Lett. **96**, 257201 (2006); Phys. Rev. B **77**, 184413 (2008).
[11] Y. Wakabayashi *et al.*, Nature Mater. **6**, 972 (2007).
[12] P. Reutler *et al.*, J. Cryst. Growth **249**, 222 (2003).
[13] E. W. Plummer *et al.*, Prog. Surf. Sci. **67**, 17 (2001).
[14] C. Kittel, *Introduction to Solid State Physics* (John Wiley & Sons, Inc., New York, 2005)
[15] F. Ronning *et al.*, Science **282**, 2067 (1998).
[16] See supplementary material at http://link.aps.org/supplemental/10.1103/PhysRevLett.105.147201.
[17] Taking into account rather small magnitude of the gap ($\Delta \sim 150$ meV) and large values of the Fermi velocity ($v_F \sim 4$ eV · Å) in the case of LSMO, one may estimate the difference between the observed remnant FS and the hypothetical FS of the noninteracting metal as much smaller than $\Delta/v_F \sim 0.04$ Å^{-1}.
[18] S. V. Borisenko *et al.*, Phys. Rev. B **64**, 094513 (2001).
[19] D. S. Inosov *et al.*, Phys. Rev. Lett. **99**, 237002 (2007); D. S. Inosov *et al.*, Phys. Rev. B **77**, 212504 (2008).
[20] Y.-D. Chuang *et al.*, Science **292**, 1509 (2001); Z. Sun *et al.*, Nature Phys. **3**, 248 (2007).
[21] N. Mannella *et al.*, Nature (London) **438**, 474 (2005).
[22] Values of the tight-binding coefficients were adjusted to yield the best approximation of the band dispersion in the vicinity of the Fermi level, i.e., the input required to calculate the response of the system.
[23] We observe no significant temperature dependence of the intensity distribution in the remnant FS maps.
[24] Y. S. Lee *et al.*, Phys. Rev. Lett. **97**, 077203 (2006).
[25] T. Ishikawa, K. Ookura, and Y. Tokura, Phys. Rev. B **59**, 8367 (1999).
[26] D. S. Inosov *et al.*, Phys. Rev. B **75**, 172505 (2007).
[27] Deviation of the revealed peak position from commensurate value $\mathbf{a}^*/4 + \mathbf{b}^*/4$ is about 2%, i.e., within error bars.
[28] Generally the peak in susceptibility for the case of sufficiently large square FS sheet (like K-barrel in the present case) is located on the diagonal. As discussed in the supplementary information, this behavior is robust with respect to fine details of the band dispersion.
[29] D. E. Moncton *et al.*, Phys. Rev. B **16**, 801 (1977).
[30] The nesting of the remnant FS in LSMO, as discussed here, can be relevant to the energy gain, in contrast to the normal band insulator.
[31] D. S. Inosov *et al.*, Phys. Rev. Lett. **102**, 046401 (2009).
[32] C. de la Cruz *et al.*, Nature (London) **453**, 899 (2008); V. B. Zabolotnyy *et al.*, Nature (London) **457**, 569 (2009).
[33] A. A. Kordyuk *et al.*, Phys. Rev. B **79**, 020504(R) (2009).
[34] F. Baumberger *et al.*, Phys. Rev. Lett. **96**, 107601 (2006).
[35] H. Cercellier *et al.*, Phys. Rev. Lett. **99**, 146403 (2007).
[36] T. Yokoya *et al.*, Phys. Rev. B **71**, 140504 (2005).